Available online at www.sciencedirect.com
SCIENCE DIRECT
Polymer 46 (2005) 1857–1864
polymer
www.elsevier.com/locate/polymer

Epoxy-silica polymers as stone conservation materials

P. Cardiano[a,*], R.C. Ponterio[b], S. Sergi[a], S. Lo Schiavo[a], P. Piraino[a]

[a]*Dipartimento di Chimica Inorganica, Chimica Analitica e Chimica Fisica, University of Messina, Salita Sperone 31 S. Agata, 98166 Messina, Italy*
[b]*CNR-Istituto Processi Chimico-Fisici (sez. Messina), Via G. La Farina 237, 98123 Messina, Italy*

Received 26 November 2004
Available online 19 January 2005

Abstract

The reaction of the epoxy derivatives 2-(3,4-epoxycyclohexyl)ethyl-trimethoxysilane (ECET) and (3-glycidyloxypropyl)methyldiethoxysilane (GLYMS) with the primary amine (3-aminopropyl)triethoxysilane (ATS) leads to solids that have been investigated by means of TG-DTA, FT-Raman and FT-IR spectroscopy. Solution ^{13}C NMR and solid state FT-Raman spectra show that the oxirane ring of ECET is not involved in the epoxy-amine addition. The structure of the resulting materials consists of a siloxane network with pendant epoxycyclohexyl groups. On the contrary, when GLYMS is allowed to react with ATS, the polymeric network develops either on the organic as on the inorganic side so that the resulting materials may be viewed as silica-epoxy hybrids with organic polymer chains covalently linked to inorganic domains. Porosity, water absorption properties and dynamic contact angle measurements were used to preliminarily evaluate the efficacy of the above materials as conservation products.

Keywords: Hybrid materials; Epoxy polymers; Conservation

1. Introduction

As a consequence of the combined degradative action of natural weathering and air pollution, resulting from anthropogenic sources, culturally and historically significant stone artifacts are today exposed to risk of being irreparably lost. The only way to preserve, as long as possible, the monumental stones from the action of the above factors, which sometimes operate synergically, is the development of new materials or novel methodologies able to consolidate and/or protect decayed stones from physical, chemical and biological attacks. Notwithstanding this, the research in this field has been mainly confined to the evaluation of a series of already marketed materials, neglecting the search for new compounds. In situ polymerization [1,2], biomediated calcite precipitation inside the stone through the application of living cultures of some calcinogenic bacteria strains [3], polymeric membranes as intelligent coatings [4], colloidal oxide particles-modified consolidants [5], new perfluorurate polymers [6] and organosilicone-modified polyurethanes [7] represent the most noticeable contributes to the field of the preserving materials.

Aimed to develop new materials for the safeguard of the architectural heritage we recently turned our attention to the synthesis of hybrid silica-epoxy polymers to be used as consolidants or protectives [8,9]. These materials widely used in electronics and as hard coatings, are virtually unexplored as conservation agents and may represent good candidates for the preservation of the cultural heritage since their properties may be tuned according to specific requirements of a consolidating or protective agent. The main purpose of a consolidation treatment is to re-establish the cohesion among the stone grains without compromise its sorptivity and mechanical properties, while a protective agent must ensure a barrier through the stone surface against water penetration, which is the main responsible for deterioration phenomena, without compromise original color.

In this paper we report on the synthesis, spectroscopic and TG-DTA investigations of the solids obtained from the reaction of epoxy derivatives 2-(3,4-epoxycyclohexyl) ethyltrimethoxysilane (ECET) and (3-glycidyloxypropyl)-methyldiethoxysilane (GLYMS) with the primary amine

* Corresponding author. Tel.: +39 90 6765712; fax: +39 90 393756.
E-mail address: cardiano@chem.unime.it (P. Cardiano).

0032-3861/$ - see front matter © 2005 Elsevier Ltd. All rights reserved.
doi:10.1016/j.polymer.2005.01.002

(3-aminopropyl)triethoxysilane (ATS) (Fig. 1). These epoxy-silica materials ought to display the properties associated to epoxy polymers and silicon-containing compounds, which are among the most used stone restoration materials. In addition ECET derivatives, owing to the presence of the cyclohexane ring and the absence of aromatic unsaturations, ought to be featured by good weathering properties while the materials containing GLYMS, owing to the presence of the methyl group, ought to perform as hydrophobic materials too. Porosity, water absorption properties and contact angle measurements were used to preliminarily evaluate their efficacy as conservation materials.

2. Experimental section

2-(3,4-Epoxycyclohexyl)ethyl-trimethoxysilane (ECET), (3-glycidyloxypropyl)methyldiethoxysilane (GLYMS), and (3-aminopropyl)triethoxysilane (ATS) were purchased from Fluka and used as received. ^{1}H and ^{13}C NMR spectra were performed in $CDCl_3$ with a Bruker AMX R-300 spectrometer operating at 300.13 and 75.47 MHz, respectively. FT-IR spectra were obtained on Perkin-Elmer RX-I on KBr disks. Micro-Raman measurements have been performed on the samples using a HR 460 Jobin Yvon spectrometer equipped with a cooled CCD detector; an Olympus BX41 microscope in confocal configuration realizes the focussing and the collecting optics; a notch filter was used in the optical geometry for the rejection of elastically scattered component. A wavenumber calibration using the silicon peak ($519.5 \pm 1\ cm^{-1}$) before measurements has been performed. Raman spectra were collected with the following operational conditions: an He/Ne laser excitation at 632.8 nm was used, the laser power at the source was of 30 mW, but the optical trajectory reduced it considerably; an X50 objective was used and the integration time ranged from 6 up to 15 s under several repetitive scans. The elastic Rayleigh line was filtered by holographic notch filters before reaching the detector. For all the samples a number of measurements, covering a spectral range of $1800 \div 500\ cm^{-1}$, were performed in order to verify their similarity. A particular regard was used in the treatment of $1320 \div 1230\ cm^{-1}$ spectral data. Exact peak positions were determined using a fitting software package (PeakFit 4, AISN Soft. Inc.), assuming a convoluted Gaussian–Lorentzian peaks profile. Thermogravimetric analyses were performed by means of Perkin-Elmer Pyris Diamond TG-DTA in the temperature range between 25 and 800 °C, under nitrogen or air atmosphere (50 mL/min) and heating rate of 10 °C/min. In some cases, in order to gain a better resolution of the superimposed DTG signals, the measurements have been carried out also with a heating rate of 5 °C/min but no significant improvements have been observed. As a consequence PeakFit 4 was employed to obtain the exact onset temperatures from DTG curves using a convoluted Gaussian signals profile. The conservation experiments were performed by treating two selected lithic samples, namely the Mistretta quartzite (MIS) and the Comiso calcarenite (COM), stones different for mineralogical features, chemical composition and porosity (porosity = 8.3 and 19.1%, respectively). The samples were allowed to adsorb the four mixtures (ECET/ATS 2:1 and 5:1, and GLYMS/ATS 2:1 and 5:1 in an ethanolic 20% solution) by capillarity (6 h) and by total immersion (24 h). Then the samples were stored for 2 months in a controlled environment (50% RH and 30 °C) to ensure evaporation of the solvent and absorption of the critical amount of water necessary to effect the hydrolysis of the Si(OR) groups. Each experiment was performed on five sets of cubic samples of $3 \times 3 \times 3$ cm carefully washed with deionized water and dried at 60 °C up to constant weight (36 h). Then water absorption tests, both as capillarity and total immersion, were performed following Normal recommendations [10]. In particular, for the capillary absorption tests, dried samples have been weighted and put in a vessel containing a 1 cm thick filter paper pile immersed in water up to the half of its height with the treated surface in contact with the paper. At fixed intervals of time, the specimens have been extracted and weighted after sponging them by a wet cloth to eliminate excess water drops. The capillarity water absorption by wicking method was performed suspending the lithic samples to the hook of the Wilhelmy balance. Moving down the hook one of the lithic sides was kept in contact with water surface [11]. The lateral sides of the cubic samples were covered with silicone to hinder the water absorption along the perimeter and to obtain capillarity rise only by the proper side. The mass variation of the samples has been automatically recorded by a computer, as a function of time. Mercury intrusion porosimetry measurements on treated stone samples were carried out with low-pressure (400 KPa) and high-pressure (200 MPa) Pascal porosimeters Fisons Instruments following the Normal recommendations [12]. The porosimetric data were taken from experiments performed on three specimens of different weight for each sample, being the weight dependent on the porosity of the stone. Dynamic contact angle measurements were performed on glass microscopy slides ($26 \times 76 \times 1$ mm by Prestige) using the Wilhelmy method by means of KSV Sigma 700 tensiometer

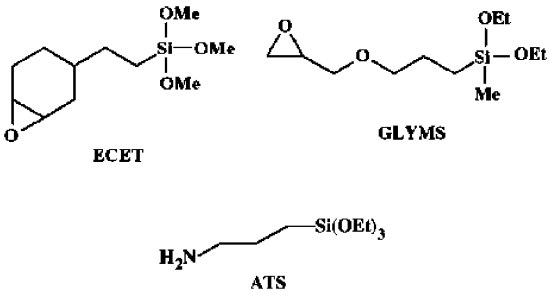

Fig. 1. ECET, GLYMS and ATS.

at the speed of 2 mm/min in Ultra Pure water (measured surface tension: 70.33 ± 0.08 mN/m). Four experiments have been performed on each coated glass slide. Furthermore, in order to show the wetting effect of water on the samples' surfaces, five continuous immersion/emersion cycles have been carried out on each coated specimen, but no significant variation in the contact angle has been detected.

3. Results and discussion

Since ECET and GLYMS possess two reactive functional groups, two main reactions may occur when reacted with ATS: (a) oxirane rings opening by addition of the hydrogen of the primary amine ATS; (b) cross-linking through polycondensation of the silanole groups generated by hydrolysis of the $Si(OR)_3$ fragments under the basic conditions provided by ATS.

As a general route the synthesis of the polymers has been accomplished by reacting, at 22 °C and 50% RH, the epoxide species ECET or GLYMS with the primary amine (3-aminopropyl)triethoxysilane (ATS) at 2:1 and 5:1 molar ratios. Then the reaction mixtures were allowed to slowly take the necessary water to effect hydrolysis of the alkoxy groups directly from air moisture and cured at room temperature. Longer gelation times and a high degree of cross-linking appear as the effects of these experimental conditions. As long as the moisture is excluded from the reaction mixture inorganic cross-linking does not occur [13,14].

When a mixture of 4 mmol of ECET and ATS (at molar ratios of 2:1 (**1**) and 5:1 (**2**), respectively), is left on standing for 20 days in a Petri dish it remains liquid if stored in a closed vessel while it solidifies in a few days, until the formation of a rubbery solid, when exposed to air. The sols were poured in glass containers and sealed with parafilm. After six days several pinholes were made in the parafilm and the volatiles allowed to slowly evaporate leading, after 20 days, to homogeneous and visually transparent solids. As previously found, ^{13}C NMR and Raman spectroscopy provide useful tools to detect the epoxy consumption [9] and the hydrolysis reaction. Samples from the reaction mixtures were taken every 24 h until the liquid phase was present, dissolved in $CDCl_3$ and analyzed by j-mod pulse sequence ^{13}C NMR spectroscopy. The spectra, even after 15 days, exhibit the four resonances (51.49, 51.59, 52.31 and 52.81 ppm) of the two carbon atoms involved in the oxirane ring (ECET consists of a mixture of isomers [15] due to the presence of three stereogenic centers), virtually unchanged. The peak at 44.83 ppm, due to the carbon in α position to the nitrogen of ATS, is unchanged too suggesting that the amino group of ATS does not behave as a reactive group. At the same time, the $Si(OMe)_3$ groups signal of ECET, centered at 50.42 ppm, gradually disappears being replaced by the peaks of the hydrolysis products $RSi(OCH_3)_{3-x}(OH)_x$ ($x=$ 1, 2, 3). The hydrolysis reaction was also followed by means of ^1H NMR by monitoring the decrease in the proton resonance of the OCH_3 groups at 3.45 ppm and the increase of the resonance of free methanol (3.30 ppm). The decrease of the OCH_3 resonance is associated with the growth of two peaks centered at 3.43 and 3.40 ppm attributable to the stepwise hydrolysis of the $Si(OCH_3)_3$ fragments. A similar trend has been found for ATS $Si(OEt)_3$ groups although both ^{13}C and ^1H spectra show, as usual, that the hydrolysis occurs at a lower rate with respect to $Si(OMe)_3$ fragments. After $\sim$20 days the formation of insoluble material, very likely due to condensation processes, prevents further solution spectra.

The ^{13}C and ^1H NMR spectra strongly suggest that the reaction proceeds through hydrolysis and polycondensation of the $Si(OR)_3$ groups while the amino group of ATS is unable to open the epoxide ring. To support this suggestion ECET was reacted with *n*-butylamine. Once again ^1H and ^{13}C NMR spectra do not show evidence of epoxy ring opening. The inertness of the oxirane ring may be due to the twisted boat conformation of the fused three- and six-membered rings of the cyclohexyl-epoxide fragment. In this conformation the axial and equatorial protons of the cyclohexane ring protect the reactive site from nucleophilic attack [16].

The solids obtained by reacting ECET and ATS, after curing at room temperature for 2 months, were examined by FT-IR and Raman spectroscopy. In the absorption domain of the IR spectra ranging from 1000 to 1200 cm^{-1} two broad absorptions culminating at 1030 and 1115 cm^{-1}, clearly due to the Si–O–Si stretching, are observed while the epoxy breathing, that in ECET appears at 880 cm^{-1}, cannot be confidently detected owing to the presence of superimposed signals. According to solution NMR investigations, FT-Raman spectra of solid **1** and **2** show virtually unchanged the band at 1267 cm^{-1}, due to the epoxy breathing. In contrast, the spectra of both the mixtures, in the $400 \div 700$ cm^{-1} range, do not show the strong polarized bands of unhydrolyzed $Si(OC_2H_5)_3$ of ATS as well as the ones of $Si(OCH_3)_3$ groups of ECET, that in the parent complexes fall at 651 and 643 cm^{-1}, respectively. Signals due to partially hydrolyzed groups $RSi(OR)_{3-x}(OH)_x$ ($x=$ 1, 2, 3) are absent too. The whole of the solution ^{13}C NMR, FT-μ-Raman and FT-IR data suggest that the growth of the polymeric network of **1** and **2** is mainly due to hydrolysis and polycondensation of the alkoxy groups of both the reactants with formation of siloxane moieties while the chemical inertness of the oxirane ring of ECET towards the amino group of ATS limits the polymer growth on the organic side.

Although at first sight the reaction of GLYMS with ATS appears similar to that previously described, it follows a different course independently from the molar ratio. To 4 mmol of (3-glycidyloxypropyl)methyldiethoxysilane in bulk was added ATS at 2:1 (**3**) and 5:1 (**4**) molar ratios following the same experimental procedures already

described. Ring opening of the epoxy group (and hydrolysis of the alkoxy groups) of GLYMS were monitored by following the disappearance, in the ^{13}C NMR spectra, of the methylene protons in α position to the nitrogen of ATS, centered at 44.83 ppm, and the bands at 44.05 and 50.65 ppm, due to the CH_2 and CH fragments of the epoxide ring of GLYMS. The spectra clearly show that in the 2/1 mixture the epoxy groups consumption was not complete until the end of NMR experiments as determined by the presence of the above signals, although considerably reduced in intensity. At the same time the absorption at 44.83 ppm, due to the carbon in α position to the nitrogen of ATS, is fully turned over suggesting that complete involvement of the amine in the ring opening reaction. In the frequency range 60÷75 ppm the spectra also exhibit sharp bands at 73.20 and 73.14 ppm attributable to a β carbon of a diol group associated to two absorptions at 68.17 and 67.68 ppm, falling in the inverted region of the spectrum, due to a α carbon diol group [17]. No bands attributable to oligo- or poly(ethyleneoxide) derivatives were detected. As far as the GLYMS inorganic part is concerned, the hydrolysis reaction of the $Si(OEt)_2$ groups occurs at a lower rate with respect to ATS triethoxy fragments. The peak at 9.82 ppm (GLYMS methylene group in α position to the silicon nuclei) and the signal at −5.04 ppm (GLYMS methyl group bonded to silicon) are in fact slowly replaced by new bands at −2.99 and at 57.40 ppm, indicating the formation of Si(OEt)(OH) moieties. The reduced hydrolysis rate of the $Si(OEt)_2$ groups may be explained in terms of electronic and steric effects. The methyl group bonded to the silicon atom, due to the positive inductive effect, increases the electronic density on the above atom disfavoring the nucleophilic attack at the silicon center with respect to trialkoxy derivates. Furthermore, according to the model of a pentacoordinated transition state operating during the base catalyzed hydrolysis of the trialkoxy silicon fragments [18], the steric hindrance of the methyl group attached to silicon disfavors the access to pentacoordinated transient species.

The spectrum of the 5/1 mixture is slightly different. As found for the lower ratio mixture the signal at 44.83 ppm due to the carbon in α position to the nitrogen of ATS gradually disappears and, after 3 days, is no more detectable. As expected the signals of the epoxy groups appear sharp and well detectable even after 15 days. While the inorganic part of GLYMS behaves as before, significant differences between the spectra of the 2/1 and 5/1 mixtures are detected in 66.51÷73.90 ppm range only. The absorptions at 73.20 and 73.14 ppm and 68.17 and 67.68 assigned to a β carbon of a diol and carbon diol groups gradually decrease and broaden. At the same time an absorption at 73.88 ppm, attributable to oligo- or poly(ethyleneoxide) derivatives, grows up [17].

As previously found for **1** and **2**, Raman spectra were very helpful to gain microstructural information and verify the involvement of the reactive sites of GLYMS and ATS in the polymeric network growth of **3** and **4**. In particular, while the inplane expansion and contraction of the ring bonds is visible as a strong polarized signal at 1257 cm^{-1} in the starting compound, it appears considerably lowered but still present in the spectra of **3** and **4**. The content of uncleaved oxirane ring, after curing for 2 months at room temperature, was estimated by curve-fitting of the experimental profile (Figs. 2 and 3). Normalization was achieved by using, as internal standard, the band at 1612 cm^{-1}, whose scattered intensity does not change as a function of the time. The experiments provide clear evidence that the

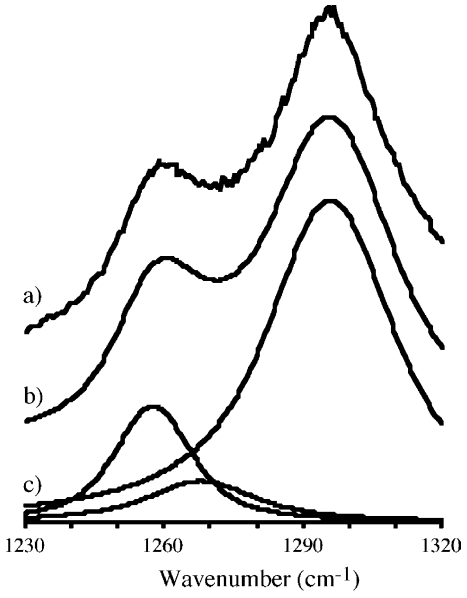

Fig. 2. Raman spectrum of sample **3** (a); global (b) and single peak (c) fitting curves obtained with PeakFit.

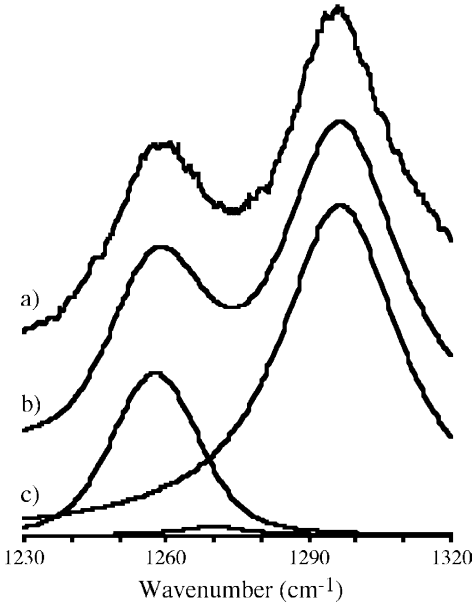

Fig. 3. Raman spectrum of sample **4** (a); global (b) and single peak (c) fitting curves obtained with PeakFit.

Table 1
Thermogravimetric results obtained for ECET/ATS and GLYMS/ATS mixtures in the temperature range of 25 ÷ 800 °C, under nitrogen flow (50 mL/min)

	1	2	3	4
First event				
T_{init} (°C)	429	427	371	370
$T_{\nu_{max}}$ (°C)	484	485	426	420
ΔM (%)	55.0	57.5	69.0	78.1
Residual mass				
Res. 800 °C (%)	40.9	40.3	26.8	16.8

reaction of the epoxy (3-glycidyloxypropyl)methyldiethoxysilane with the primary amine (3-aminopropyl)triethoxysilane proceeds with a remarkable high percentage (92 and 88% for **3** and **4**, respectively) of cleaved rings. As far as the inorganic fragment is concerned, the spectra of **3** and **4** do not exhibit the $\nu(SiO_3)$ absorption at 651 cm^{-1}, characteristic of ATS, nor the bands due to $\nu(SiO_2)$ of GLYMS at 637 and 613 cm^{-1} showing that, differently from the solution mixture, due to the long stay at room temperature of **3** and **4**, in the solid state unhydrolyzed or partially hydrolyzed silicon alkoxide groups are no more present. It is worth to mention that solids featured by the same Raman and thermal properties as **1**–**4** were obtained performing the reactions in dry ethanol.

Thermal behavior and thermal stability of **1**–**4** were investigated through TG-DTA experiments. The weight changes during heat-treatment in nitrogen or air and other relevant data are shown in Tables 1–3 and Figs. 4 and 5. The thermal behavior patterns of **1**–**4** in dynamic nitrogen show the following common features, endothermic in nature: (i) a low-temperature step in the range 130 ÷ 137 °C, not reported in Table 1, corresponding to the removal of small quantity of residual condensation volatiles, water or alcohols, produced during the curing phase or following the cooking during the thermoanalysis; (ii) the main decomposition process, occurring in the range 420 ÷ 485 °C, related to the thermal stability of the investigated mixtures; (iii) a few percent thermogravimetric step, found only for **4**, detected at 299 °C very likely due to small quantity of unreacted GLYMS. The comparison between the ECET/ATS thermograms in nitrogen shows a common behavior also in terms of weight loss and degradation rate, while, as far as GLYMS/ATS blends are concerned, **4** shows a faster and higher main weight loss (78.1%) as compared to **3** (69%). The different complexity between the network of **3** and **4** mixtures is also confirmed by the unusual low residual mass found for **4**. In fact, while the residual mass at 800 °C of **3** is in good agreement with the calculated SiO_2 percentage, sample **4** shows a residual mass lower (16.8%) with respect to the theoretical value (24.4%), suggesting the formation of organosilicon volatiles species [19].

Higher degradation temperature, lower decomposition rate and weight loss are the thermogravimetric parameters of ECET/ATS blends as compared to GLYMS/ATS blends. The combined thermogravimetric data suggest that the mixtures containing the epoxy derivative 2-(3,4-epoxycyclohexyl)ethyl-trimethoxysilane are featured by a different complexity and higher stability of the network than those containing (3-glycidyloxypropyl)methyldiethoxysilane.

To verify the thermal stability of **1**–**4** and their residues in an oxidative environment the thermogravimetric

Table 2
Thermogravimetric results obtained for ECET/ATS mixtures in the temperature range of 25 ÷ 800 °C, under air flow (50 mL/min)

	1	2
First event		
T_{init} (°C)	250	237
$T_{\nu_{max}}$ (°C)	276	243
ΔM (%)	5.0	4.8
Second event		
T_{init} (°C)	178	179
$T_{\nu_{max}}$ (°C)	339	340
ΔM (%)	21.1	28.6
Third event		
T_{init} (°C)	375	396
$T_{\nu_{max}}$ (°C)	396	415
ΔM (%)	10.8	7.3
Fourth event		
T_{init} (°C)	390	410
$T_{\nu_{max}}$ (°C)	571	570
ΔM (%)	23.6	23.6
Residual mass		
Res. 800 °C (%)	36.3	34.1

Table 3
Thermogravimetric results obtained for GLYMS/ATS mixtures in the temperature range of 25 ÷ 800 °C, under air flow (50 mL/min)

	3	4
First event		
T_{init} (°C)	239	230
$T_{\nu_{max}}$ (°C)	274	299
ΔM (%)	14.2	16.6
Second event		
T_{init} (°C)	188	174
$T_{\nu_{max}}$ (°C)	327	319
ΔM (%)	34.7	39.5
Third event		
T_{init} (°C)	418	400
$T_{\nu_{max}}$ (°C)	592	584
ΔM (%)	9.2	6.2
Residual mass		
Res. 800 °C (%)	38.4	33.4

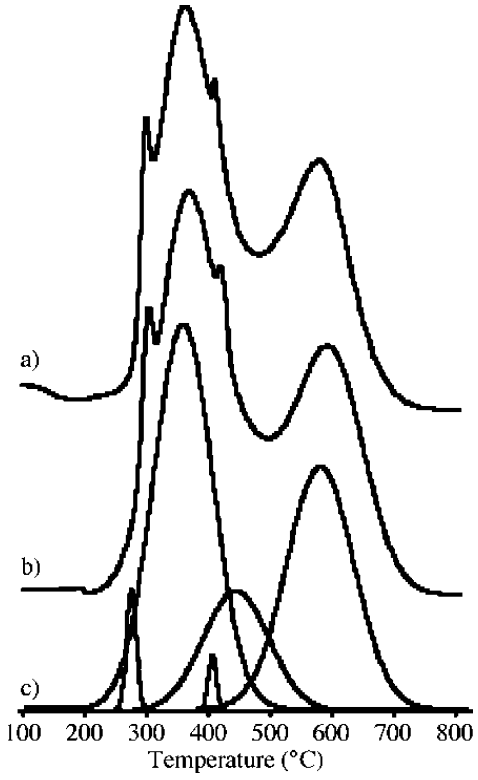

Fig. 4. DTG curve of sample **1** under air flow (a); global (b) and single peak (c) fitting curves obtained with PeakFit.

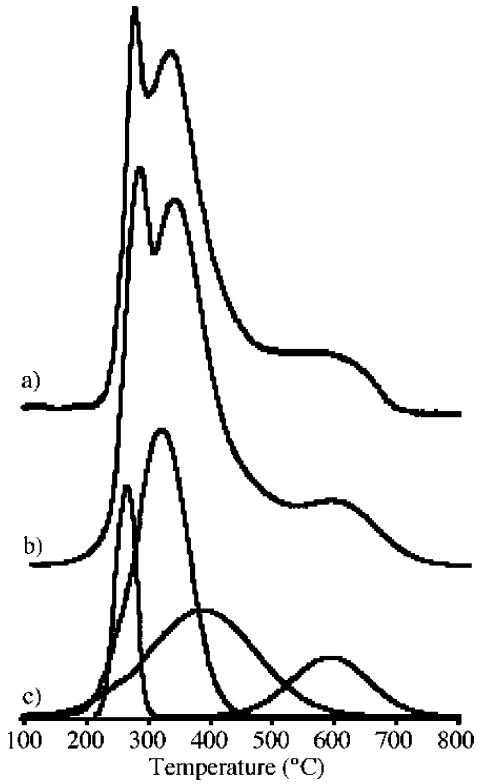

Fig. 5. DTG curve of sample **3** under air flow (a); global (b) and single peak (c) fitting curves obtained with PeakFit.

experiments were also carried out in air. No specific differences were detected during heating in presence of oxygen between the blends containing ECET although, at first sight, the thermooxidative behavior of **1** and **2**, in the temperature range 250÷350 °C, appears different. Blend **1** in the above range exhibits two well distinct degradation steps, with T_{max} of 276 and 339 °C, and weight losses of 5 and 21.1%, respectively. As far as **2** is concerned, in the same range the DTG curve shows only a single broad signal featured by a total weight loss of 33.4% and a T_{max} of 340 °C. In order to compare the DTG signals of **1**–**2** in the same temperature range, the deconvolution of the whole curves was performed. After fitting and deconvolution, it appeared clear that the events occurring during heating of the two ECET/ATS blends are comparable although they only differ for the intensity of the main signals. Furthermore, the simulated DTG curves showed also the presence of a fifth slow degradation step (not considered in the Table 2), with a T_{max} of 447 °C, almost unrecoverable from the experimental data (Fig. 4). Noteworthy both **1** and **2** show an important, low rate, degradation process with T_{max} at ~570 °C. This high-temperature process (less evident for **3** and **4**) could be due to combustion of some polymeric residue not previously oxidized. However, we are inclined to believe that, following initial oxidation of the organic fragment bonded to the silicon atoms and as a consequence of the large number of silicon atoms reacting with oxygen, the formation of new, highly cross-linked siloxane domains may account for the above high-temperature degradation step. The shift of the weight loss curves to lower temperatures, with respect to the investigations carried out in nitrogen, was also observed when the samples containing GLYMS are heated in the presence of oxygen. The decomposition of **3** occurs in three main events, namely at 274, 327 and 592 °C (Table 3); the first two steps are characterized by a comparable rate, while the last process is featured by a very low rate of decomposition. The thermooxidative decomposition of **4** is quite similar although the first two steps cannot be clearly distinguished, as they appear superimposed. Once again deconvolution of the DTG signals showed that the degradation processes occurring both for **3** and **4**, in the temperature range 260÷340 °C, are similar even if featured by a different intensity. The deconvolution showed also the presence of a hidden process with a T_{max} 390 °C in both cases (Fig. 5). The residual masses measured at 800 °C are higher with respect to data obtained under nitrogen flow suggesting the occurrence of complementary reactions rather than simple combustion. In fact, nitrogen atoms incorporated in a silicate network as well as alkyl substituted silicon alkoxy derivatives may produce oxycarbides [20] or oxinitrides [21].

*3.1. Dynamic contact angle and hydrophobic properties of **1–4***

Since the wettability of a stone sample plays a determinant role in weathering phenomena, one of the requirements to be fulfilled in artistic stone conservation is

the protection of the stone surface against water penetration. The unique and commonly used solution is the treatment of the stone surface with water repellent materials. With this in mind, the hydrophobic properties and hence wettability of **1**–**4** were tested by means of advancing and receding contact angle. Owing to the highly scattered data obtained on stones, due to the surface heterogeneity, porosity and roughness, the experiments were carried out on glass slides coated by the polymers.

Notwithstanding the presence of hydrophobic alkyl and cyclohexyl groups the water repellence activity of **1**–**4** does not raise much enthusiasm. The advancing contact angles of **1** and **2**, 88 and 92.3°, respectively, reflect the higher content of epoxycyclohexyl groups present in **2** while an opposite trend is observed for **3** and **4** that display contact angles of 83.8 and 79.2°, respectively. As far as receding contact angle is concerned, it ranges from 45.6° for **4** to 56.8° for **2**. It is worth to mention that static and advancing contact angles data lead to misleading interpretations when measured on porous substrates as they allow only to detect the presence of a water-repellent product on the sample surface rather than to assess the degree of protection of a stone [22]. On the contrary the receding contact angle is viewed as a better parameter for the evaluation of the effectiveness of a protective treatment since the stone surface heterogeneity as well as the micro roughness play an important role in determining the resulting angle thus allowing to obtain more accurate value of the protection degree [23]. Since contact angle measured on coated glasses cannot exceed the one measured on the treated stone sample, we deduce that **1** and **2** only may represent an acceptable barrier to water when applied on stone.

The presence of hydrophilic fragments such as unreacted amino groups (for **1** and **2**), Si–O–Si (**1**–**4**) and oxirane fragments (**1**–**4**) negatively affects the samples surface properties suggesting that the above groups, beside to ensure adhesion to the stone surface, provide, at the air interface, both hydrophilic and hydrophobic domains. So the water repellency due to the methyl or cyclohexyl groups is counterbalanced by hydrophilic fragments on the solid surface. According to this suggestion the measurements also display hysteresis values ranging from 33.6 to 38.5°, as expected when hydrophobic and hydrophilic fragments are present.

Despite the previous conclusions, coating of the two selected lithotypes, COM and MIS, with **1**–**4** results in a water shielding effect as determined by capillarity and total immersion water absorption tests. The capillarity absorption tests were made according to the Normal recommendations and by the Wilhelmy balance. The adoption of the procedures published by the Normal Commission leads to suggest that ECET/ATS mixtures exert on COM stone an excellent barrier against water penetration (absorbed water reduction values at saturation higher than 93%) while, between the GLYMS/ATS mixtures, **3** only exerts a good waterproofing behavior, during the first 24 h of the test. The soaking activity of the less porous MIS stone, when treated with **1**–**4**, is much less affected by the treatment. Data gathered in Figs. 6 and 7 show that contrasting results are obtained when the capillarity absorption tests are performed by the Wilhelmy balance. The water absorbed by wicking is in fact greater than that measured by the Normal procedure. As suggested by Brugnara et al. [11] the wicking method provides a more precise description of the water absorption process since it does not require, as Normal procedure does, several manual operations. So capillarity absorption tests made according to Normal recommendations should be carefully reconsidered. Total immersion tests, carried out according to the appropriate Normal protocol, confirm that all the mixtures but **4** represent a suitable barrier against water penetration inside COM pores. Their strong protecting activity does not appreciably decreases by the time remaining excellent until saturation occurs. As far as the low porosity stone is concerned, **3** and **4** are unable to significantly reduce its absorption properties while **1** and **2** mixtures represent a good water barrier at the beginning of the test only.

Independently from the method, water absorption tests would suggest that **1** and **2** represent ideal candidates to inhibit water penetration inside the pore network of medium porosity stones. Contact angle investigations lead to less enthusiastic conclusions. These contrasting results may be explained assuming that, beside to exert water repellent activity, **1** and **2** fill the pores of the stones so decreasing the voids that water can occupy. To verify this suggestion porosimetric investigations were carried out on the two lithotypes, after impregnation with **1**–**4**.

The impregnation of the two stones with mixtures containing ECET and GLYMS leads to a decrease of the total porosity ranging from 20% (for the less porous stone) to 31% for the higher porosity one. Furthermore all the treatments induce few variations on the pore size distributions of Comiso stone while the shifting of the average

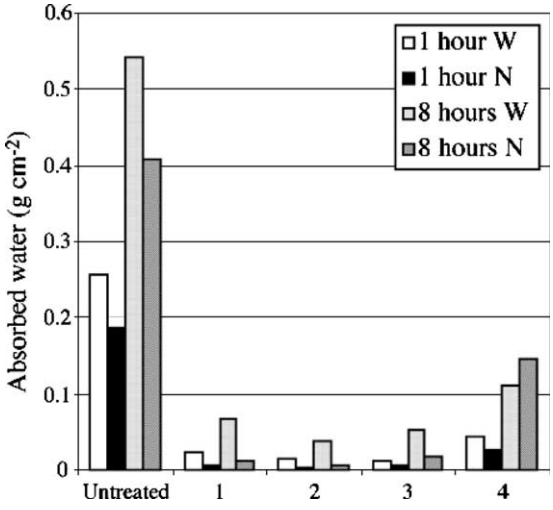

Fig. 6. Capillarity water absorption measured by wicking (W) and Normal (N) method on COM samples treated with **1**–**4**.

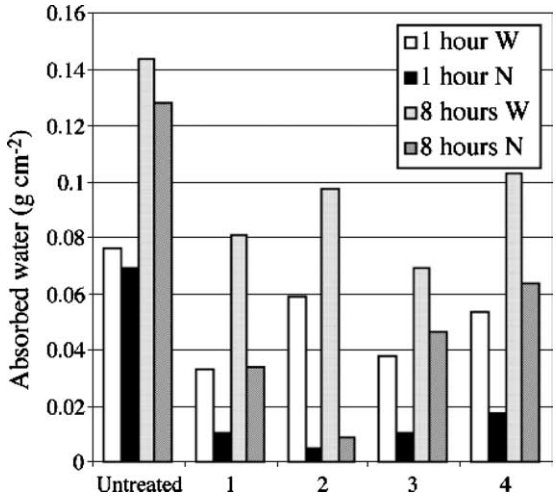

Fig. 7. Capillarity water absorption measured by wicking (W) and Normal (N) method on MIS samples treated with **1**–**4**.

pore radius toward smaller pores is dramatic on MIS as the impregnation with all the mixtures causes the partial filling of the pores ranging from 1 to 0.5 μm to give the maxima between $0.4 \div 0.3$ μm. These data suggest that the noticeable reduction of the water absorbed by the higher porosity stone is due to two combined effects: improvement of the water repellent properties of the stone following the treatment with **1**–**4** and reduction of porosity.

4. Conclusions

Although we cannot make speculations on structure and length of **1**–**4**, some conclusions may be drawn. The polymerizable monomer 2-(3,4-epoxycyclohexyl)ethyltrimethoxysilane (ECET) and (3-glycidyloxypropyl)methyldiethoxysilane (GLYMS), functionalized by $Si(OR)_3$ groups, may react either via addition of the aminic protons of (3-aminopropyl)triethoxysilane (ATS) leading to the polymerization of the organic fragment or, via hydrolysis and further polycondensation of the silanole groups, leading to siloxane domains. Solution ^{13}C NMR and solid state FT-Raman spectra show that the oxirane ring of ECET does not undergo addition reactions. So the structure of **1** and **2** consists of a siloxane polymeric network with pendant epoxycyclohexyl groups. In contrast, when GLYMS is allowed to react with ATS, independently from the sequence, both the above reactions occur. As a consequence the polymeric network develops either on the organic as on the inorganic side and the resulting materials **3** and **4** may be viewed as hybrid silica-epoxy polymers with organic polymer chains covalently linked to inorganic domains. The structural differences reflect the thermal stability and, to a lesser extent, the water repellent activity of **1**–**4**. Compounds **1**–**3**, and less **4**, despite unfavorable contact angle values, provide a powerful barrier against water penetration into the more porous stone while they appear unsatisfactory when applied on low porosity stones.

Acknowledgements

This work was supported by the Ministero dell'Istruzione, dell'Università e della Ricerca (Miur), Italy.

References

[1] Vicini S, Margutti S, Princi E, Moggi G, Pedemonte E. Macromol Chem Phys 2002;203:1413–9.
[2] Cardiano P. Ann Chim (Rome) 2003;93:249–56.
[3] Tiano P, Biagiotti L, Mastromei G. J Microbiol Methods 1999;36:139–45.
[4] Drioli E, Gagliardi R, Donato L, Checchetti A. J Membrane Sci 1995;102:131–8.
[5] Aggelakopoulou E, Charles P, Acerra ME, Garcia AI, Flatt RJ, Scherer GW. Mater Res Soc Symp Proc 2002;712:15–20.
[6] Alessandrini G, Aglietto M, Castelvetro V, Ciardelli F, Peruzzi R, Toniolo L. J Appl Polym Sci 2000;76:962–77.
[7] Puterman M, Jansen B, Kober H. J Appl Polym Sci 1996;59:1237–42.
[8] Cardiano P, Sergi S, Lazzari M, Piraino P. Polymer 2002;43:6635–40.
[9] Cardiano P, Mineo P, Sergi S, Ponterio RC, Triscari M, Piraino P. Polymer 2003;44:4435–41.
[10] (a) Normal Protocol 11/85. Assorbimento d'acqua per capillarità. Coefficiente di assorbimento capillare. Rome: CNR-ICR; 1986. (b) Normal Protocol 7/81. Assorbimento di acqua per immersione totale. Capacità di imbibizione. Rome: CNR-ICR; 1981.
[11] Brugnara M, Degasperi E, Della Volpe C, Maniglio D, Penati A, Siboni S, et al. Colloid Surface A 2004;241:299–312.
[12] Normal Protocol 4/80. Distribuzione del volume dei pori in funzione del loro diametro. Rome: CNR-ICR; 1980.
[13] Brinker CJ, Scherer GW. Sol–gel science: the physics and chemistry of sol–gel processing. Boston: Academic Press; 1990 pp. 802–19.
[14] Ochi M, Takahashi R, Terauchi A. Polymer 2001;42:5151–8.
[15] Udagawa A, Yamamoto Y, Chujo R. Polymer 1990;31:2425–30.
[16] Soucek MD, Abu-Shanab OL, Anderson CD, Wu S. Macromol Chem Phys 1998;199:1035–42.
[17] Templin M, Wiesner U, Spiess HW. Adv Mater 1997;9:814–7.
[18] Riegel B, Blittersdorf S, Kiefer W, Hofacker S, Muller M, Schottner G. J Non-Cryst Solids 1998;226:76–84.
[19] Mutin PH. J Sol-Gel Sci Technol 1999;14:27–38.
[20] Soraru GD. J Sol-Gel Sci Technol 1994;2:843–8.
[21] Hampshire S. J Non-Cryst Solids 2003;316:64–73.
[22] Toniolo L, Della Volpe C, Brugnara M, Poli T. Mater Res Soc Symp Proc 2002;712:91–7.
[23] Della Volpe C, Penati A, Peruzzi R, Siboni S, Toniolo L, Colombo C. J Adhes Sci Technol 2000;14:273–99.